Effect of Chemical Oxidation on the Structure of Single-Walled Carbon Nanotubes

Jin Zhang,*,† Hongling Zou,† Quan Qing,† Yanlian Yang,† Qingwen Li,† Zhongfan Liu,*,† Xinyong Guo,‡ and Zuliang Du‡

Center for Nanoscale Science and Technology (CNST), College of Chemistry & Molecular Engineering, Peking University, Beijing 100871, P. R. China, and Laboratory of Lubrication and Functional Materials, Henan University, Kaifeng 475001, P. R. China

Received: November 20, 2002; In Final Form: February 12, 2003

In the present study, we report the systematic investigation of the effect of chemical oxidation on the structure of single-walled carbon nanotubes (SWNTs) by using different oxidants. The oxidation procedure was characterized by using infrared spectroscopy and transmission electron microscopy (TEM). The SWNTs were produced by chemical vapor deposition (CVD) and oxidized with three kinds of oxidants: (1) nitric acid (2.6 M), (2) a mixture of concentrated sulfuric acid (98 wt %) and concentrated nitric acid (16 M) (v/v = 3/1) and (3) $KMnO_4$. The results reveal that the different functional groups can be introduced when the SWNTs are treated with different oxidants. Refluxing in dilute nitric acid can be considered as a mild oxidation for SWNTs, introducing the carboxylic acid groups only at those initial defects that already exist. The abundance of the carboxylic acid groups generated with this oxidant remained constant along with the treating time. In contrast, sonication of SWNTs in H_2SO_4/HNO_3 increased the incidence of carboxylic acid groups not only at initial defect sites but also at newly created defect sites along the walls of SWNTs. Compared to the two oxidants above, when $KMnO_4$ in alkali was used as the oxidant, which is relatively mild, different amounts of −OH, −C═O, and −COOH groups were introduced. The oxidation processes begin mainly with the oxidation of the initial defects that arise during the CVD growth of the SWNTs and are accompanied by processes that can be roughly divided into two steps: (1) the defect-generating step and (2) the defect-consuming step. Specifically, during the defect-generating step, the oxidants attack the graphene structure by electrophilic reactions and generate active sites such as −OH and −C═O. This step depends on the oxidant's ability to generate −C−OH groups and to transform them into −C═O groups. During the defect-consuming step, the graphene structure of the tube was destroyed by the oxidation of the generated active sites in step 1. The defect-consuming step mostly counts on the ability of the oxidant to etch/destroy the graphite-like structure around the already generated −C═O and their neighborhood groups.

Introduction

Carbon nanotubes, in particular, single-walled carbon nanotubes (SWNTs) have attracted the attention and interest of researchers in many fields because of their remarkable properties.[1] They are expected to have numerous applications, for example, flat panel field-emission displays, nanoelectronic devices, chemical sensors, batteries, ultrasharp nanoprobes for scanning probe microscopy, nanotweezers, actuators, and so forth.[2−11] Initial studies have indicated that chemical functionalization of the open ends and the walls of SWNTs would play a vital role in tailoring their properties and applications.[12] In the tubular structure of SWNTs, each carbon atom is joined to three neighbors, so the bonding is essentially sp^2. However, there may be a small amount of sp^3 character due to the curvature, such as the pentagons and heptagons existing in the end cap and on the side of the tube, and defects on the tube's surface as well. Different defects make for various chemical structures that are relatively active, such as the pentagon−heptagon pair defects or the tube−tube junctions, the Stone−Wales defect (the bond rotation), substitutional impurities, structural deformations caused by bending or twisting of the nanotubes and vacancies on the wall, and so forth. Thus, it would be possible and somewhat convenient to functionalize the SWNTs in a chemical way.[13−20] However, functionalizing nanotubes is, if anything, rather more difficult than, for example, assigning functional groups to the ends or walls of the nanotubes and properly characterizing them.

Liu et al. reported the first use of a 3:1 concentrated H_2SO_4/HNO_3 mixture to cut the highly tangled long ropes of SWNTs into short, open-ended pipes and thus produced many carboxylic groups at the open end.[21] The oxidation of carbon nanotubes with HNO_3, O_3, $KMnO_4$, OsO_4, and RuO_4 was also reported soon afterward.[22−26] As a result of the chemical oxidation, the ends and walls of the nanotubes are covered with oxygen-containing groups such as carboxylate groups, ether groups, and so forth.[27−31] The presence of oxygenated groups on nanotubes is important both to the fundamental research of nanotubes and to their applications in electronic devices. In our recent work,[32] we developed a wet chemical approach for organizing randomly tangled SWNTs into well-ordered arrays on gold and silver surface using a self-assembly technique in which the as-prepared SWNTs were cut into short pipes by chemical oxidation using H_2SO_4/HNO_3, allowing the nanotubes to be terminated by carboxyl functionalities. Then the shortened SWNTs can be immobilized on $-NH_2$-terminated self-assembled monolayers

* Corresponding authors. E-mail: jzhang@chem.pku.edu.cn. E-mail: lzf@chem.pku.edu.cn. Tel and Fax: 86-10-6275-7157.
† Peking University.
‡ Henan University.

10.1021/jp027500u CCC: $25.00
Published on Web 03/27/2003

(SAMs) surfaces.[33] This achievement is an important step toward the construction of nanodevices using carbon nanotubes.

To get a more systematic view of the chemistry of the chemical oxidation of SWNTs, it is necessary to understand the chemical processes of the treatment in more detail. Raman and near-infrared (NIR) spectroscopy are very useful in this regard.[34−35] Kuznetsova et al. have recently reported the chemical structure of oxygen-containing functional groups on SWNTs by using near-edge X-ray absorption fine strucuture (NEXAFS) and vibrational spectroscopy,[30] which indicate that both carbonyl (C═O) and ether R−O−R functionalities are present when the tube is purified and cut with either HNO_3/H_2SO_4 or H_2O_2/H_2SO_4 mixtures. Thermal decomposition of carboxyl and quinone functional groups formed by acidic cutting of the SWNTs was investigated by FTIR, in which CO, CO_2, CH_4, and H_2 were evolved during the thermal treatment.[29] Douglas and co-workers have reported FTIR spectroscopic studies of the oxidation and etching of SWNTs using ozone at 298 K and of the subsequent thermal stability of the oxygenated groups.[36]

In view of the difficulties in understanding the structural transformation during the chemical oxidation, more specifically, the transitional and the resultant chemical structure, we have tried to follow the oxidation processes by using infrared spectroscopy and transmission electron microscopy (TEM). In the present study, we systematically investigated the effect of chemical oxidation using 3:1 concentrated H_2SO_4 (98 wt %)/HNO_3 (16 M) mixtures, HNO_3 (2.6 M), and $KMnO_4$ oxidants on the structure of SWNTs with the aid of infrared spectroscopy and TEM. The results indicate that the oxidation processes begin mainly with the oxidation of the initial defects that arise during the CVD growth of the SWNTs and are accompanied by processes that can be roughly divided into two steps: (1) the defect-generating step, and (2) the defect-consuming step. Specifically, during the defect-generating step, the oxidants attack the graphene structure by electrophilic reactions and generate active sites such as −OH and −C═O. This step depends on the oxidant's ability to generate −C−OH groups and to transform them into −C═O groups. During the defect-consuming step, the graphene structure of the tube was destroyed by the oxidation of the generated active sites in step 1. The defect-consuming step mostly counts on the ability of the oxidant to etch/destroy the graphitelike structure around the already generated −C═O and their neighborhood groups.

Experimental Section

1. Preparation of Carbon Nanotube Samples. SWNTs were prepared in a simple CVD setup made of a tube furnace and gas flow control units with nanosize MgO as the support; the purity of the sample reached 90%.[37] In a typical growth experiment, about 1 g of catalyst was put into an alumina boat inside a quartz tube and was heated to the reaction temperature under Ar flow at a flow rate of 250 mL/min. The reaction began when methane gas was input and directed with Ar into the tube. The growth reaction lasted for some desired time (typically 30 min), and then the methane gas was turned off and the furnace was cooled to room temperature under an Ar atmosphere. The as-prepared SWNTs sample was first treated with 37% hydrochloric acid to remove the catalyst and support material and then sonicated in 0.2% Triton X-100 solution (pH 10), followed by microfiltration with a 1.2-μm-pore membrane under vacuum. A typical Raman spectrum of the prepared SWNTs is shown in Figure 1. For SWNTs, four Raman bands are strongly resonance-enhanced. Three of them are located around 1600 cm^{-1}, corresponding to the characteristic A_{1g}, E_{1g}, and E_{2g} modes of the graphene sheet, and the fourth strong band appears around 200 cm^{-1}, which is unique to single-wall nanotubes and arises from the radial breathing mode (RBM), which indicates that the prepared SWNTs have a diameter of 1.1 nm.[34,38] The inset of Figure 1 is a typical SEM image of the tube after purification.

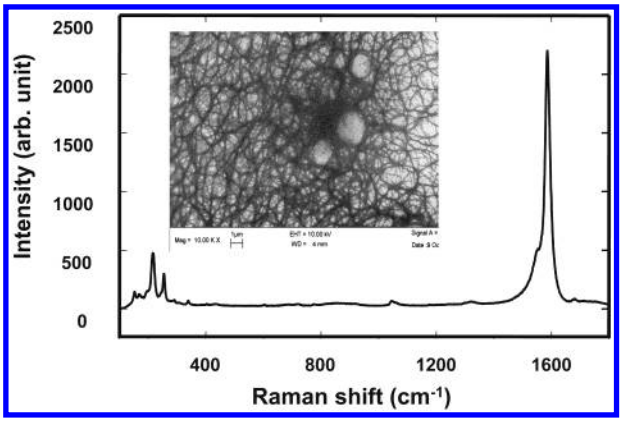

Figure 1. Raman spectrum and SEM image of purified SWNTs.

2. Oxidative Treatment of SWNTs. Three different oxidants were employed to treat the purified SWNTs. The oxidation processes were as follows:

2A. 2.6 M HNO_3. In a typical procedure, approximately 80 mg of a purified sample of nanotubes was refluxed in 50 mL of 2.6 M HNO_3 for 48 h. The solid was collected on a 100-nm-pore membrane filter and rinsed with deionized water.

2B. Potassium Permanganate. A purified sample of nanotubes (50 mg) was first refluxed in 30 mL of an alkalescent solution of potassium permanganate (0.2 M $KMnO_4$ and 0.2 M NaOH) for 40 min, and then 1.5 g of Na_2SO_3 was added with stirring, followed by an addition of l5 mL of 1 M H_2SO_4. The obtained solution was filtered with a 100-nm-pore membrane under vacuum in dilute NaOH and then in deionized water. In the final step of rinsing, dilute HCl was added to protonate the terminated groups of SWNTs.

2C. Concentrated H_2SO_4/HNO_3 Mixture (3:1). In a typical example, 60 mg of purified SWNT was suspended in 50 mL of a 3:1 mixture of concentrated H_2SO_4(98 wt %)/HNO_3(16 M) and sonicated in a water bath for 24 h. The resultant suspension was then diluted with 250 mL of water, and the SWMTs were collected on a 100-nm-pore membrane filter and washed with deionized water.

3. Characterization of Carbon Nanotubes. TEM, SEM, and IR were employed to characterize all CVD-grown samples and oxidative treated samples. TEM was performed on a Hitachi H810 at 20 kV; sample preparation involved sonicating materials in deionized water for at least half an hour and then putting a drop of the resulting suspension onto a carbon film supported by copper grids. SEM was conducted at 25 kV using a Hitachi H-800 field-emission instrument. To prepare samples for SEM, the treated materials were sonicated in 1,2-dichloromethane for 10 min, and a drop of the suspension was placed onto a silicon substrate and allowed to evaporate. FTIR spectra were measured on a Nicolet AVATAR-360 FT-IR spectrophotometer with a liquid-N_2-cooled MCT detector.

Results and Discussion

1. Infrared Spectrocopy. For the sake of chemical decoration and modification of carbon nanotubes, we should first open the caps of the nanotubes and thus obtain certain active chemical

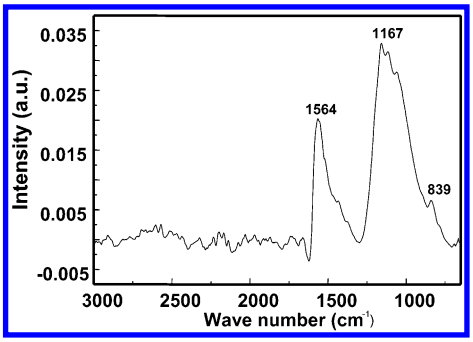

Figure 2. Typical FTIR spectrum of the as-prepared SWNTs.

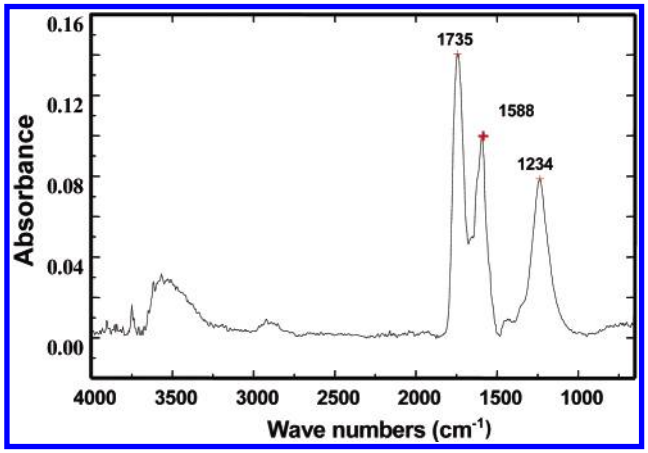

Figure 3. Typical FTIR spectrum of SWNTs treated with the acid mixture for 2 h.

groups. The oxidants we have tried include dilute HNO_3, $KMnO_4$ in alkali solution, and a mixture of H_2SO_4 (98 wt %) and HNO_3 (16 M). These methods are all effective in opening the nanotubes but are very different in oxidation ability. The abundance of the funtional groups and the length distribution of the SWNTs after treatment also vary. Dilute HNO_3 can purify the SWNTs and etch the tube from the terminal and the defects in the side wall, but such a relatively mild oxidant cannot generate abundant functional groups. Similarly, in the case of using $KMnO_4$ in alkali solution as a moderate oxidant, the tube is not effectively opened. However, as shown below, the acid mixture is strong enough to break the tube and generate an abundance of functional groups.

Theoretical investigation reveals that monocrystalling graphite belongs to the D^4_{6h} space-group symmetry. Thus, an out-of-plane A_{2u} mode around at 868 cm^{-1} and an in-plane E_{1u} mode around at 1588 cm^{-1} are infrared-active.[39,40] A typical FTIR spectrum of the as-prepared SWNTs by CVD is shown in Figure 2. We found the A_{2u} mode around at 839 cm^{-1} and the E_{1u} mode at 1564 cm^{-1} with a broadened peak. Similar to the reference, we also found a peak around 1200 cm^{-1} in Figure 2, even it does not yet have a clear assignment.

1A. FTIR Spectroscopy of the H_2SO_4/HNO_3 Treated Sample. Normally, the acid mixture is used to purify as-prepared SWNTs. After treatment, the tubes are not only cut into short pipes but also purified because the acid mixture is known to intercalate and exfoliate graphite. A typical FTIR spectrum of SWNTs treated with the acid mixture for 2 h is shown in Figure 3, in which a new peak around 1735 cm^{-1} appears. It is normally assigned to the C═O-strength vibration in the COOH group,[29] which means that the acid-mixture treatment will introduce some C═O groups to the end or the side of the SWNTs. It is interesting that we found that the peak around 1735 cm^{-1} shifted from 1737 cm^{-1} to 1720 cm^{-1} as the time of the treatment

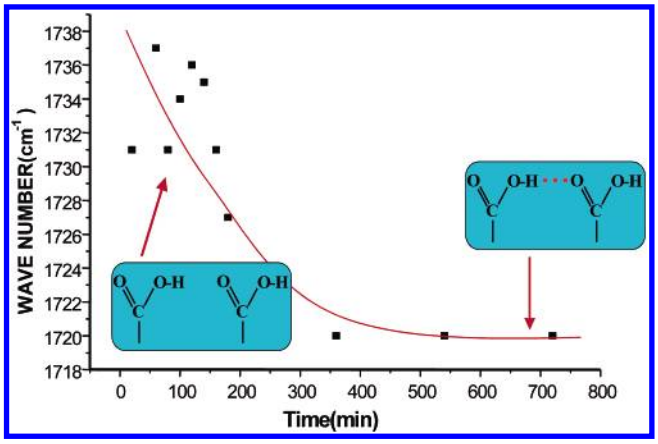

Figure 4. Relationship between the peak position (−COOH) and treating time.

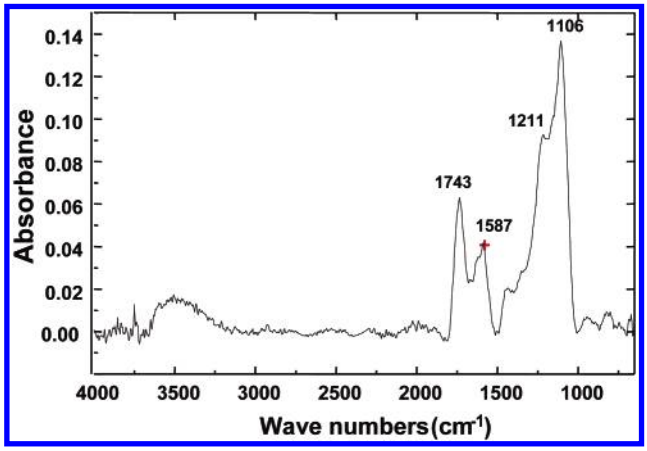

Figure 5. Typical FTIR spectrum of SWNTs treated with the HNO_3 for 48 h.

increased (Figure 4), which suggested that the abundance of −COOH groups increased along with the treatment time. Meanwhile, the formation of hydrogen bonds between the −COOH groups became more effective. Compared with the as-prepared SWNTs in Figure 2, we also found that in the treated SWNTs the peak originally around 1564 cm^{-1}, which is assigned to the −C═C− groups, shifted to a higher frequency around 1588 cm^{-1}, which may suggest a change in the structure of the SWNTs.

1B. FTIR Spectra of SWNTs Refluxed in HNO_3 (2.6 M). Similar to the acid mixture, HNO_3 is also used to purify the SWNTs on the basis of its selective oxidation of carbon amorphism. A dilute nitric acid reflux digests the surfactant, and in the meantime, it etches the carbonaceous particles that are shelled off from the SWNTs and thus further purifies the SWNTs. Because of the relatively higher reactivity of the caps and some defects in the side walls of the nanotubes, SWNTs are also consumed during this process, which results in partial opening of the tubes. Figure 5 shows the typical FTIR spectrum of the SWNTs refluxed in HNO_3 for 48 h. Compared with the as-preapred SWNTs, a new peak around 1740 cm^{-1} appeared and can be assigned to the C═O group of −COOH in the free state. This issue will be discussed later in this article. At treatment times up to 96 h, we observed that the peak did not shift (Figure 6). This suggested that prolonged refluxing of SWNTs in dilute HNO_3 cannot generate more −COOH groups at the end or the side of the tubes because if it had done so the more abundant −COOH would have been able to form hydrogen bonds more effectively, which should have caused the peak to

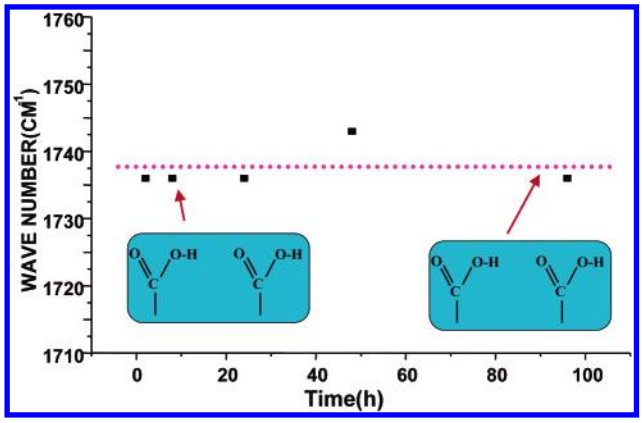

Figure 6. Relationship between the peak position (−COOH) and treating time.

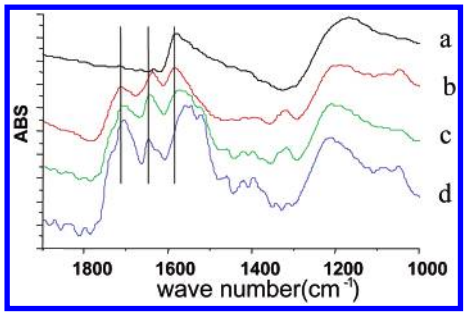

Figure 7. FTIR spectra of SWNTs with $KMnO_4$ in alkali for different times: (a) original sample; (b) 10 min; (c) 40 min; (d) 70 min.

red shift, as could be observed in the results of the other two oxidation procedures. In other words, after 2.6 M HNO_3 consumed the already existing defects, it could not etch into the aromatic rings of the tube, thus lacking the ability to generate more −COOH groups or "cut" the tubes, as can be observed with TEM.

1C. FTIR Spectra of SWNTs Treated with $KMnO_4$. The reference showed that ozone etching can introduce some C═O groups (quinone) to the ends or side walls of SWNTs.[24] However, such a situation could not be observed in either of the experiments treating the SWNTs with HNO_3 or with H_2SO_4/HNO_3, even for a very short time (data not shown). To reveal the oxidation process, we tried $KMnO_4$ in alkali as the oxidant, which is relatively a mild oxidant compared to the other two and shows a controllable regular oxidation degree as we change the reaction time. Figure 7 showed the selected region of FTIR spectra of the treated SWNTs in which we found two new peaks around 1740 and 1640 cm^{-1}; these can be assigned to C═O in COOH and in quinone, respectively. As the oxidation proceeded, the ratio of the area of the peak at 1740 cm^{-1} to the area of the peak at 1640 cm^{-1} increased. These indicate that the quinone groups may be an intermediate in the oxidation process and may keep being transformed to −COOH in a further step. Moreover, the peak at around 1575 cm^{-1}, which can be assigned to the stretching mode of −C═C− groups, showed a shift to lower frequency along with the treatment, which also suggests some structural change in the side wall of the tube.

1D. Evidence of COOH Groups Created by Chemical Oxidation. The stretching vibration mode of the C═O group in aromatic acid often appears in the range of 1690−1660 cm^{-1} in FTIR spectra.[41] This peak position remains below 1700 cm^{-1} even when −COOH is in the free state. However, after the chemical oxidation using three kinds of oxidants, the peak that should be assigned to the stretching vibration mode of C═O in COOH always appeared higher than 1720 cm^{-1},[27] which falls into the typical range of the stretching vibration mode of C═O in COOR or even higher. It is from COOH or COOR? What caused it go up to such a high frequency? We did two simple experiments to confirm the state of C═O.

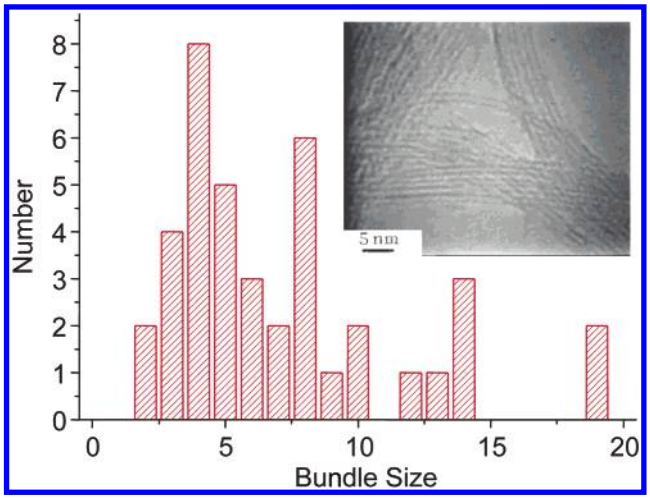

Figure 8. Distribution of bundle size and typical TEM image of SWNTs.

First, the oxidized nanotubes are sonicated in 0.1 M NaOH solution for 5 min, centrifuged, dried, and then analyzed with FTIR. The FTIR spectra were very different from those before the treatment: the peak near 1710 cm^{-1} disappeared, and two new peaks at around 1540−1615 cm^{-1} and 1640 cm^{-1} were found, which is clear proof of $-COO^-$ and thus confirms the original existence of −COOH. (See Supporting Information.)

Second, we intermingled the oxidized SWNTs with some benzene carbonic acid to determine if there would be any interaction between the −COOH groups of these two substances. (See Supporting Information.) The oxidized SWNTs were sonicated in a benzene carbonic acid ethanol/water solution, centrifuged, and then dried. The concentration of the benzene carbonic acid is controlled at a certain level so that in the FTIR spectrum it is not a main contribution in the area of interest. We assume that, as for the signals given by the benzene carbonic acid, the relative height of the peaks at 1454, 1425, and 1692 cm^{-1} do not change during the process and the first two peaks can be used to judge how much benzene carbonic acid has been added to the tubes. In comparing the two Figures, we can say that in the mixture the peak assigned to −C═O at 1692 cm^{-1} is mainly the signal given by −COOH on the tubes because we can estimate the contribution of the benzophenone from the remaining 1454- and 1422-cm^{-1} peaks. Thus, the result of this experiment agrees with our opinion that the shift to a higher wavenumber of the −C═O group in FTIR is the result of the inefficiency in forming hydrogen bonds. We will discuss this issue later in this paper.

2. TEM Investigation. TEM provides sufficient resolution that it can be used to obtain some direct visualization of the length or diameter distribution and the defects. In our observation, the SWNTs tend to exist as bundles, which is agreement with the references. Figure 8 shows the histogram of the bundle-size distribution of SWNTs under TEM. The SWNTs produced by CVD with MgO support have a typical bundle size of 6 nm (Figure 8). A detailed analysis of the TEM images showed that the proportion of individually existing SWNTs was about 5%, as a statistical result of 650 nanotubes in 30 TEM images. Most of these individual SWNTs have a smooth or unique structure (inset of Figure 8). In addition, we also found some nanotubes with defects on the side wall and one opened-end tube in a

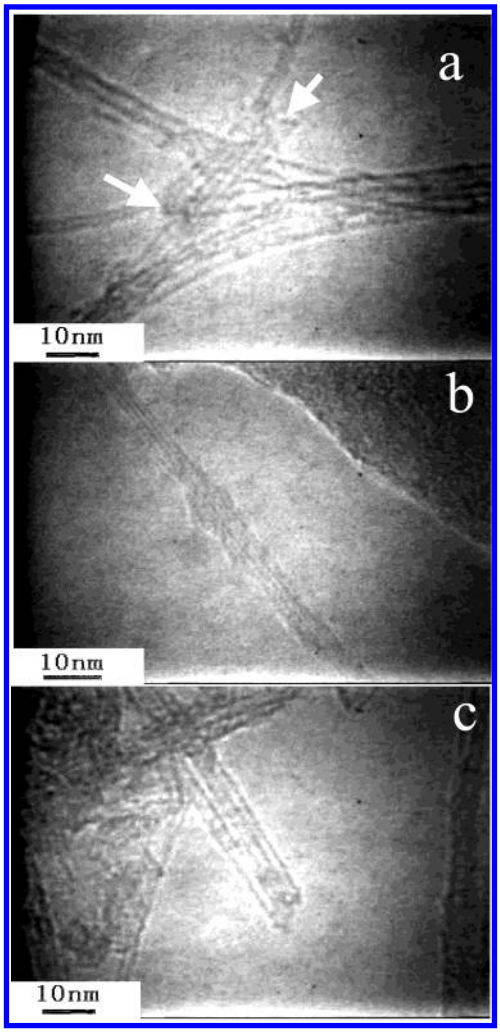

Figure 9. Typical TEM images of SWNTs treated with different oxidants: (a) acid mixture (the arrows point to the open ends of tubes); (b) HNO_3; (c)KMnO4.

bundle (Figure 9a). This open end provides a reactive site to the reagent, for example, the oxidants. After treatment with H_2SO_4/HNO_3, more individual SWNTs appeared under TEM. The tubes' ends were opened, and some new defects were generated on the tubes' surface as well. Most interesting, we found this simple treatment to be a powerful and simple way to enrich the large-diameter SWNTs. We found that this proportion became remarkably increased upon increasing the oxidation time in the acid mixture, reaching ca. 20% after 96 h of treatment.[42] These phenomena will help us to explain the oxidation mechanism. As for the treatment by HNO_3, the typical length of the SWNTs was similar to that with the as-prepared SWNTs. Several typical high-resolution TEM images showed very rough surfaces of SWNTs compared with those of the untreated samples (Figure 9b), which may indicate a different oxidation mechanism. However, in the case of $KMnO_4$ in alkali treatment, the opening was not effective at all. A typical TEM image is shown in Figure 9c, in which more impurity and byproduct were observed. It was very hard to get a clear view of the tubes, and most of them were long. We could see some tube ends opened and some closed, which indicates that the oxidation ability of $KMnO_4$ in alkali is relatively weak.

3. On the Mechanism of Oxidation. The problems concerning the reactive position of functionalization and the existent state of groups after oxidative treatment as well as the mechanism of oxidative shortening are still under study. To design proper experiment to modify nanotubes and to fabricate polymers or composites based on SWNT, we have tried to understand the structural change and reaction process that occur during chemical oxidation by tracking variations in SWNTs with infrared and electron spectroscopy. In the following section, we discuss some aspects of the mechanism of the oxidation process in SWNTs.

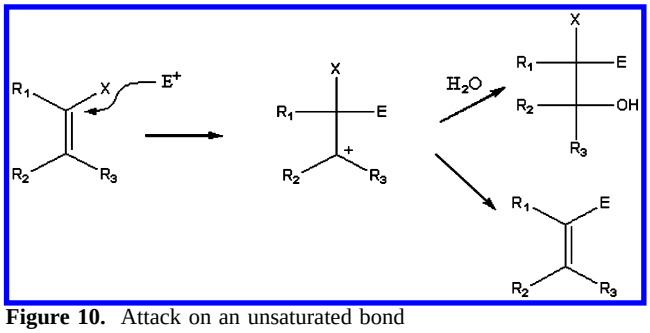

Figure 10. Attack on an unsaturated bond

Attacking Location. Generally, we tend to consider that the reaction is easy to start at the defect sites because of the heavy strain of the hexagon−heptagon pairs or that it begins by the attack on remaining CH and CH_2 groups that may be a natural result of the CVD process. But we noticed that when we treated the tubes with the acid mixture more indentations and nicks than we expected were introduced into the walls of nanotubes and many of the tubes were cut into short pipes. These data show that the oxidant not only attacks defects but also takes action on the relatively integrated graphene structures. In fact, we consider the electrophilic attack on the borderline between hexagons or on the exposed edges of hexagons to be a main contribution to the −COOH and −OH groups rather than the reactions induced by those initial defects arising during CVD growth.

There are many similar reactions such as the oxidation of anthrene and phenathrene, in which the reactants assail places 9 and 10, and the electrophilic addition reaction of C_{60},[43] in which the active position lies on the borderline between two hexagons but not between a pentagon and a hexagon. Furthermore, we think that the hexagon electrophilic reaction actually cut the tubes down to short pipes. Because of the rigorous conditions used during oxidation, there may appear in the side of the tube open holes that are formed by microscopic domains of high temperature produced by ultrosonication, thus providing more attacking locations.

Process of Oxidative Reaction. The structures of nanotubes synthesized by the CVD method are highly complex, so the reaction process may be full of possibilities. The pentagon, heptagon, or larger ring lying in the tubes leads to alterations in the shape and chirality of tubes. They also bring in unsaturated and dangling bonds. These segments may terminate with CH, CH_2, and other radicals and ions and may bring a large tensile force and break the aromaticity of rings, hence making the oxidation easier. After these parts are consumed, the aromatic rings are opened by electrophilic reaction, thus the shortening process begins. First, the electrophilic reagent attacks C═C, producing hydroxyl (Figure 10). Then, the hydroxyl is converted to a quinone group, as in the cases of anthrene and phenanthrene, or broken up to −COOH in a stronger oxidative environment. However, if we want to get quinone into the carbon tube, two hydroxyls should be in the neighborhood, as in the case of the oxidation of anthrene; otherwise, a long-distance electron transfer would maintain the aromaticity of the tube, which would be rather energetically disadvantageous. This is coincident with the fact that we observe only the quinone group when we use

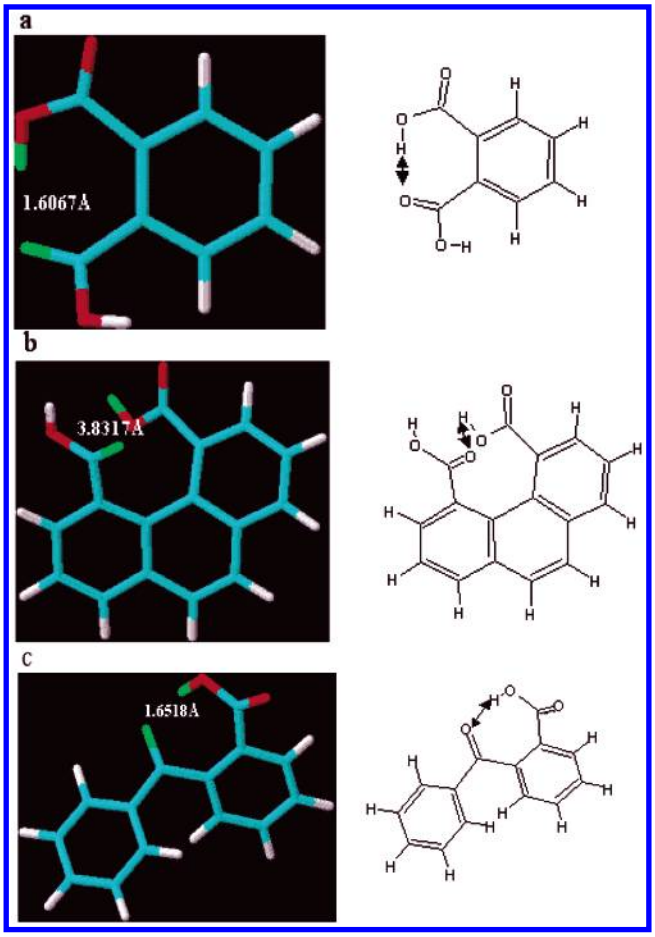

Figure 11. Calculated distance between the hydrogen atom and the nearby oxygen atom: (a) two −COOH groups on the same benzene ring; (b) two −COOH groups on different benzene rings; (c) −COOH next to a −C═O bridge.

$KMnO_4$ as the oxidant but not in other cases because $KMnO_4$ is more capable of making ortho hydroxyls. In the cases of other oxidants, we find very little evidence of the quinone groups even if we decrease the reaction time.

In the meantime, we found that although the acid mixture and dilute nitric acid both introduce the carboxyl group, the strength vibration peaks are not at the same location. This phenomenon will be discussed specifically below, but here an obvious fact should be taken into account that the acid mixture can easily produce NO_2^+, which is a strong electrophilic reagent producing hydroxyl groups easily and hence generating more −OH and −COOH groups, thus contributing to the decrease of strength vibration peaks below 1720 cm^{-1}, as described in the next section.

Outcome of Oxidative Reaction. No matter what kinds of structures are used—the pentagon, heptagon, larger rings, or other reductive groups—only these groups can show up after strong oxidative treatment: −COOH, −OH, and C═O. At the same time, these groups must be connected with the aromatic rings directly, and C═O can lie only in the plane of the ring or on the bridging C atom of the intersected rings.

Deduction of Stereo Conformation after Oxidative Reaction. To determine the efficiency of the formation of hydrogen bonds of various structures, we calculated some simulation molecules as follows. And we can see from the result that ortho −COOH on the same hexagon or −COOH next to a −OH or −C═O can form a hydrogen bond efficiently but in other cases cannot (Figures 11 and 12).

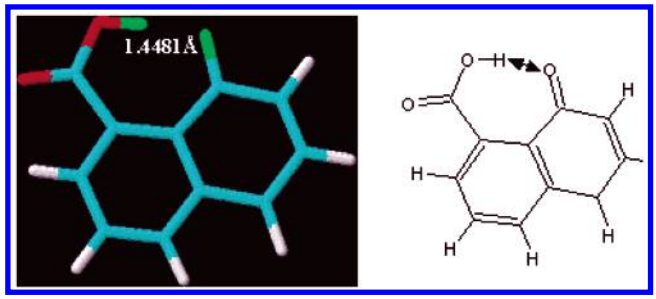

Figure 12. Calculated distance between the hydrogen atom and the nearby oxygen atom for −COOH next to −C═O on the nearest benzene ring.

However, a −COOH next to a −C═O has little chance to occur because we have just now argued that the −C═O group is more likely to appear geminately on the same ring.

According to the results of the experiment, we can see that in most cases the −COOH group's positions is in agreement with that shown in Figure 11b (inefficient in forming a hydrogen bond). That is to say that they exist on different rings. A possible explanation for this is the following: To form an ortho −COOH structure, we have to cut at least four bonds, but to form the structure in Figure 11b, at the most three have to be cut, not to mention the passivating effect that the first formed −COOH would have on the ring to which it belongs. Meanwhile, although we believe that the formation of −OH is a precursor to −COOH, the later oxidation can hardly form a −COOH near another −OH because of the possible electronic or steric effects.

Conclusions

We present a systematic investigation of the effect of chemical oxidation on the structure of single-walled carbon nanotubes (SWNTs) by using different oxidants: nitric acid (2.6 M), a mixture of concentrated sulfuric acid (98 wt %) and nitric acid (16 M) (v/v = 3:1), and $KMnO_4$. The results reveal that different functional groups can be introduced when the SWNTs are treated with different oxidants.

The process of the oxidation of SWNTs can be described as follows:

(1) An initial attack on the original existing active sites such as the $-CH_2$ and −CH groups and heptatomic rings, which carry a large strain force, is carried out. This is primarily how the oxidation begins.

(2) Later or maybe concurrently with step 1, electrophilic addition begins at hexatomic−hexatomic boundaries, generating more active sites or rather new defects. We tend to consider −OH to be the most common intermediate result. We may call this a defect-generating step.

(3) Under strong oxidation conditions, the graphene structure around the already generated active sites is broken, and the tube is cut off. We may call this a defect-consuming step.

The latter two steps compete and cooperate with each other, and the defect-generating step is much faster than the defect-consuming step.

$KMnO_4$ is very good at generating new defects, which can be seen from the IR results of very short time treatment, whereas dilute HNO_3 needs long-time refluxing to have an effect on the tubes. Nevertheless, it can hardly generate new defect sites by attacking 6-6 ring boundaries and limits its effect only for large strain sites and reducing groups, as can be seen in the IR results in which the frequency of the −C═O stretch remains constant for different time treatments. In other words, the dilute HNO_3 does not go into steps 2 and 3 after it finishes step 1. The acid mixture, because of the existence of concentrated H_2SO_4,

effectively produces electrophilic groups such as NO_2^+ and thus can attack −C═C− much easier. This is the same case as for another oxidant we have tried: piranha (H_2SO_4 (98 wt %) + H_2O_2 (30 wt %), data not shown here), which can generate OH^+.

$KMnO_4$ and dilute HNO_3 are all inefficient in the defect-consuming step whereas the acid mixture or the piranha is strong enough to cut the graphite structure. And as the treatment time increases, we get more −COOH and −OH with the acid mixture, which lowers the frequency of the −C═O stretch.

Acknowledgment. We are grateful for financial support from the National Natural Science Foundation of China (NSFC 59910161982, 29973001, 30000044, 90206023) and the Ministry of Science and Technology of China (2001CB6105).

Supporting Information Available: FTIR spectra of oxidized SWNTs after sonication in 0.1 M NaOH and benzene carbonic acid after being mixed with oxidized SWNTs. This material is available free of charge via the Internet at http://pubs.acs.org.

References and Notes

(1) (a) Ebbesen T. W.; Lezec H. J.; Hiura H.; Bennett J. W.; Ghaemi H. F.; Thio T., *Nature* **1996**, *382*, 54 (b) Odom, T. W.; Huang, J. L.; Kim, P.; Lieber, C. M. *J. Phys. Chem. B* **2000**, *104*, 2794−2809.

(2) de Heer, W. A.; Chatelain, A.; Ugarte, D. *Science* **1995,** *270*, 1179.

(3) Choi, W. B.; Jin, Y. W.; Kim, H. Y. et al. *Appl. Phys. Lett.* **2001,** *78*, 1547

(4) Wang, Q. H.; Setlur, A. A.; Lauerhaas, J. M.; Dai, J. Y.; Seeling, E. W.; Chang, R. P. H., *Appl. Phys. Lett.* **1998,** *72*, 2912.

(5) Saito, S. *Science* **1997**, *278*, 77

(6) Tans, S. J.; Verscheueren, A. R. M.; Dekker: C. *Nature* **1998,** *393*, 49.

(7) Lefebvre, J.; Antonov, R. D.; Radosavljevic, M. et al. *Carbon* **2000**, *38*, 1745.

(8) Haggenmueller, R.; Gommans, H. H.; Rinzler, A. G. et al. *Chem. Phys. Lett.* **2000**, *330*, 219.

(9) Jin, Z.; Pramoda, K. P.; Xu, G.; Goh, S. H. *Chem. Phys. Lett.* **2001**, *337*, 43.

(10) Ajayan, P. M.; Schadler, L. S.; Giannaris, C.; Rubio, A. *Adv. Mater*. **2000**, *12* 750.

(11) Wong, S. S.; Harper, J. D.; Lansbury Jr., P. T. et al. *J. Am. Chem. Soc.* **1998**, *120*, 603.

(12) (a) Ausman, K. D.; Piner, R.; Lourie, O.; and Ruoff, R. S.; Korobov, M., *J. Phys. Chem. B* **2000**, *104(38)*, 8911. (b) Bahr, J. L.; Mickelson, E. T.; Bronikowski, M. J.; Smalley, R. E.; Tour, J. M. *Chem. Commun*. **2001**, *2*, 193.

(13) Hiura, H.; Ebbesen, T. W.; Fujita, J.; Tanigaki, K.; Takada, T. *Nature* **1994**, *367*, 148.

(14) Liu, M.; Cowley, J. M. *Carbon* **1994**, *32*, 2**,** 393.

(15) Stone, A. J.; Wales, D. J. *Chem. Phys. Lett*. **1986**, *128*, 501.

(16) Terrones, M.; Terrones, H. *Full. Sci. Tech*. **1996**, *4*, 517.

(17) Crespi, V. H.; Cohen, M. L.; Rubio, A. *Phys. Rev. Lett*. **1997**, *79***,** 2093.

(18) Terrones, H.; *et al. Phys. Rev. Lett.* **2000**, *84*, 1716.

(19) Chernozatonskii, L. A. *Chem. Phys. Lett*. **1998**, *297*, 257.

(20) Zou, H. L.; Yang, Y. L.; Li, Q. W.; Zhang, J.; Liu, Z. F. *Carbon* **2002**, *40*, 2282.

(21) Liu, J.; Rinzler, A. G.; Dai, H. J.; Hafner, J. H.; Bradley, R. K.; Boul, P. J.; Lu, A.; Lverson, T.; Shelimov, K.; Huffman, C. B.; Rodriguez-Macias, F.; Shon, Y. S.; Lee, T. R.; Colbert, D. T.; Smalley, R. E. *Science* **1998**, *280*, 1253.

(22) Kyotani, T.; Nakazaki, S.; Xu, W. H.; Tomita, A. *Carbon* **2001**, *39*, 782.

(23) Mawhinney, D. B.; Naumenko, V.; Kuznetsova, A. *Chem. Phys. Lett.* **2000**, *324*, 213.

(24) Mawhinney, D. B.; Naumenko, V.; Kuznetsova, A.; Yates Jr, J. T.; Liu, J.; Smalley, R. E. *J. Am. Chem. Soc.* **2000,** *122*, 2383.

(25) Hernadi, K.; Siska, A.; Thien-Nga, L. *Solid State Ionics* **2001,** *141*, 203.

(26) Hwang, K. C.*J Chem. Soc. Chem. Comm*. **1995**, *2*, 173.

(27) Tsang, S. C.; Harris, P. J. F.; Green, M. L. H. *Nature* **1993,** *362*, 520.

(28) Ajayan, P. M.; Ebbesen, T. W.; Ichihashi, T.; Iijima, S.; Tanigaki, K.; Hiura, H. *Nature* **1993,** *362*, 522.

(29) Kuznetsova, A.; Mawhinney, D. B.; Naumenko, V.; Yates Jr, J. T.; Liu, J.; Smalley, R. E. *Chem. Phys. Lett.* **2000,** *321*, 292.

(30) Kuznetsova, A.; Popova, I.; Yates, J. T., Jr.; Bronikowski, M. J.; Huffman, C. B.; Liu, J.; Smalley, R. E.; Hwu, H. H.; Chen, J. G. *J. Am. Chem. Soc.* **2001**, *123*, 10699.

(31) Li, Q. W.; Yan, H.; Ye, Y. C.; Zhang, J.; Liu, Z. F. *J. Phys. Chem. B* **2002**, *106*, 11085.

(32) (a) Liu, Z. F.; Shen, Z. Y.; Zhu, T.; Hou, S. F.; Ying, L. Z.; Shi, Z. J.; Gu, Z. N. *Langmuir* **2000**,*16*, 3569. (b) Wu, B.; Zhang, J.; Wei, Z.; Cai, S. M.; Liu, Z. F., *J. Phys. Chem. B* **2001**, *105*, 5075. (c) Nan, X. L.; Gu, Z. N.; Liu, Z. F. *J. Colloid Interface Sci.* **2002**, *245*, 311. (d) Peng, D.; Liu, Z. F.; Wu, B.; Nan, X. L.; Zhang, J.; Wei, Z. *ChemPhysChem* **2002**, *10*, 898. (e) Yang, Y. L.; Zhang, J.; Nan, X. L.; Liu, Z. F. *J. Phys. Chem. B **2002**, 106*, 4139.

(33) Chattopadhyay, D.; Galeska, I.; Papadimitrakopoulos, F. *J. Am. Chem. Soc.* **2001**, *123*, 9451.

(34) (a) Dresselhaus, M. S.; Dresselhaus, G.; Eklund, P. C. *Science of Fullerences and Carbon Nanotubes*, Academic: San Diego **1996**. (b) Rao, A. M.; Richter, E.; Bandow, S.; Chase, B.; Eklund, P. C.; Williams, K. A.; Fang, S.; Subbaswamy, K. R.; Menon, M.; Thess, A.; Smalley, R. E.; Dresselhaus, G.; Dresselhaus, M. S. *Science* **1997**, *275*, 187.

(35) Chen, J.; Hamon, M. A.; Hu, H.; Chen, Y. S.; Rao, A. M.; Eklund, P. C.; Haddon, R. C. *Science* **1998**, *282*, 95.

(36) Douglas, B. M.; Naumenko, V.; Kuznetsova, A.; Jr, J. T. Y. *J. Am. Chem. Soc.* **2000**, *122*, 2383.

(37) (a) Li, Q. W.; Yan, H.; Cheng, Y.; Zhang, J.; Liu, Z. F. *J Mater. Chem.* **2002**, *12 (4):* 1179−1183. (b) Yan, H.; Li, Q. W.; Zhang, J.; Liu, Z. F. *Carbon* **2002**, *40*, 2693. (c) Li, Q. W.; Yan, H,; Li, X. H.; Zhang, J.; Liu, Z. F. *Chem. Mater.* **2002**, *14*, 4262.

(38) Raman spectra were recorded under Ranishaw system 1000 using a 50mW He−Ne laser operating at 632.8 nm and a CCD detector in ambient atmosphere at room temperature. The final spectra presented is an average of 15 spectra recorded at different regions over the entire range of the sample.

(39) Knight, D. S.; White, W. B. *J. Mater. Res.* **1989**, *4*, 385.

(40) Kastner, J.; Pichler, T.; Kuzmany, H.; Curran, S.; Blau, W.; Weldon, D. N.; Delamesiere, M.; Draper, S.; Zandbergen, H. *Chem. Phys. Lett.* **1994**, *221*, 53.

(41) Lin-Vien, D.; Colthup, N. B.; Fateley, W. G.; Grasselli, J. G., *The handbook of Infrared and Raman Characteristic Frequencies of Organic Molecules*, Academic Press: Inc., 1991.

(42) Yang, Y. L.; Zou, H. L.; Wu, B.; Li, Q. W.; Zhang, J.; Liu, Z. F. *J Phys Chem B* **2002**, *106*, 7160.

(43) (a) Kitagawa, T.; Tanka, T.; Tanaka, Y.; Takeuchi, K.; Komatsu, K. *J. Org. Chem*. **1995**, *60*, 1490. (b) Kitagawa, T.; Tanka, T.; Tanaka, Y.; Takeuchi, K.; Komatsu, K. *Tetrahedron* **1997**, *53*, 9965.